TECHNICAL MEMORANDUMS

NATIONAL ADVISORY COMMITTEE FOR AERONAUTICS

No. 703

TAKE-OFF AND PROPELLER THRUST

By Martin Schrenk

Zeitschrift für Flugtechnik und Motorluftschiffahrt
Vol. 23, No. 21, November 14, 1932
Verlag von R. Oldenbourg, München und Berlin

Washington
April, 1933

NATIONAL ADVISORY COMMITTEE FOR AERONAUTICS

TECHNICAL MEMORANDUM NO. 703

TAKE-OFF AND PROPELLER THRUST*

By Martin Schrenk

I. INTRODUCTION

Since the fifty-ninth report of the D.V.L. (Deutsche Versuchsanstalt für Luftfahrt) (reference 1) no further German treatises on the take-off distance have appeared. Still that fundamental and meritorious work is incomplete and unsatisfactory in many respects.

In the calculation of the ground run the practical engineer is disturbed by the disproportionality between the complexity of the fundamental formula and the uncertainty of the assumptions, especially as regards the propeller thrust. Blenk develops an approximation formula, whose degree of accuracy is difficult to ascertain and which he himself designates as useful only for purposes of comparison.

This defect can be remedied by the development of an extremely simple and yet accurate formula, which makes it possible to ascertain simultaneously and directly the effect of the determinative quantities on the ground run and the effect of alterations. It is derived from the diagram of forces after deducting the friction of the ground and the resistance of the air. The assumption of the proportional decrease in the propeller thrust with the dynamic pressure, which is indispensable for every calculation, should be verified by comparison with propeller-model tests. This leads almost necessarily to the use of a non-dimensional thrust formula derived for the purpose, which can also serve well for other aviation purposes. These wider relations, however, can be treated only by way of suggestion, corresponding to the scope of the present work.

---

*"Abflug und Schraubenschub." Z.F.M., November 14, 1932, pp. 629-639.

Moreover, in the above-mentioned work, the actual flight path after the take-off was replaced by a broken line, with an arbitrary assumption (best criterion of climb) for the flight condition in climbing. Aside from the fact that the steepest climb does not take place with the best criterion of climb, the disregard of the transition arc before the climb is accompanied by considerable uncertainty. We will endeavor to calculate this arc, at least approximately.

As a result of the work, it is endeavored to obtain, along with the truest possible comprehension of the course of the thrust, a complete, simple and clear formula for the whole take-off distance up to a certain altitude, which shall give the correct relative weight to all the factors.

II. NOTATION

The notation is the same as in my previous work, with the addition of the following symbols: (Reference 2.)

P, accelerating force.

R, ground friction.

s, distance.

h, altitude at end of take-off distance.

r, radius of transition arc.

μ, coefficient of ground friction.

φ, path angle during climb.

ζ, figure of merit (Bendemann).

Φ, θ, Σ, ψ, Π, nondimensional coefficients for speed, dynamic pressure, thrust, drag, and accelerating force. All the quantities are in homogeneous units.

III. DERIVATION OF THE TAKE-OFF FORMULAS

1. Simplified Formulas for the Take-Off Run

During the ground run the airplane is subjected to the propeller thrust, air resistance, and ground friction. After deducting the last two from the propeller thrust, the remaining force serves to accelerate the airplane. Of course these deductions must be made before the formation of the differential equation, which may be expected to simplify the solution considerably.

For landplanes only the take-off distance is important, while the time consumed does not matter. It is therefore expedient to form the differential equation so as to obtain the ground run by a single integration. Such is the case when the energy equation, instead of the momentum equation, is taken as the basis. The formula then reads

$$P \, d \, s = \frac{G}{g} \, d \left(\frac{v^2}{2} \right)$$

or, with

$$\frac{v^2}{2} = \frac{q}{\rho},$$

$$d \, s = \frac{G}{\gamma} \frac{dq}{P} \qquad (1)$$

Here P is the force available for acceleration at any instant of the ground run. According to Figure 1

$$P = S - W - R$$

For the propeller thrust we choose, in agreement with Blenk, the Aleyrac assumption of linear fall with the dynamic pressure. We shall see later how far this assumption is justified. The air resistance and ground friction are proportional to the dynamic pressure in so far as the airplane runs at a constant angle of attack. For simplicity, it is first assumed that the airplane runs and rises at the same angle of attack (lift coefficient c_{a_1}). On this assumption the ground run is somewhat longer than if it were made at a more favorable coefficient of lift. In Section III,3 it will be shown how the shortest ground run can be regarded. Hence, we obtain, as shown in Figure 1, a linear course of the accelerating force P over the dynamic

pressure q of the form

$$P = P_o - \frac{P_o - P_1}{q_1} q$$

Thus equation (1) becomes

$$d s = \frac{G}{\gamma} \frac{d q}{P_o - \frac{P_o - P_1}{q_1} q}$$

and finally, by integration,

$$s = \frac{G}{\gamma} \frac{q_1}{P_o - P_1} \ln \frac{P_o}{P_1} \qquad (2)$$

This result is really quite simple. Nevertheless formula (2) is not yet clear, since the two terms

$$\frac{q_1}{P_o - P_1} \quad \text{and} \quad \ln \frac{P_o}{P_1}$$

are opposed and it is not immediately obvious as to which predominates. Hence a further simplification will be undertaken.

Instead of the linear drop from P_o to P_1, it will be assumed that the force

$$P_m = \frac{P_o + P_1}{2}$$

the mean accelerating force, will act uniformly during the whole take-off process. Consequently, equation (1) becomes

$$d s = \frac{G}{\gamma} \frac{d q}{P_m}$$

and integration yields

$$s_1 = \frac{G}{P_m} \frac{q_1}{\gamma} \qquad (3a)$$

This expression is, in fact, extremely simple and clear. Its physical significance is best perceived from the following form

$$s_1 = \frac{G}{P_m} \frac{v_1^2}{2 g} \qquad (3b)$$

in which $v_1^2/2g$ is the speed of the airplane at the instant of leaving the ground. It may therefore be said that the ground run is equal to the speed of the airplane at the instant of leaving the ground multiplied by the ratio of the weight to the mean accelerating force.

For practical use the ground run may also be expressed in the following form, from which the connection with the airplane's characteristics directly proceeds.

$$s_1 = \frac{G}{P_m}\frac{G}{F}\frac{1}{c a_1 \gamma} \qquad (3c)$$

2. Accuracy of the Approximation Formula

The hatched area in Figure 1 contains the accelerating forces P, which are determinative for the take-off. It does not correspond, however, to the ground run, since the latter was not obtained as an integral over $P\,dq$, but over dq/P. The last integral denotes the area of a figure with the reciprocal acceleration forces as ordinates. Since this figure is not a trapezoid, but is bounded on one side by a curve, its area cannot be accurately expressed by a mean ordinate P_m, and all the less so, the greater the difference between the initial and final ordinate.

The degree of accuracy of the approximation formula is found by comparing the accurate formula (2) with the approximation formula (3a) at variable P_0/P_1. We then obtain, for the ratio of an assumed true mean force P_m' (for which the formulas (3) would be exact), in addition to the arithmetical mean

$$P_m = \frac{P_0 + P_1}{2}$$

used by us, the following formula

$$\frac{P_m'}{P_m} = \frac{P_0 - P_1}{P_0 + P_1}\,\frac{2}{\ln\frac{P_0}{P_1}}$$

In the same degree as P_m' remains behind P_m, the ground run calculated by the approximation formula (3a) is also too small. From Figure 2 it follows that the resulting error is small, being less than 3 per cent in the important region below $P_0/P_1 = 2$. Moreover the error is easily corrected by using the error curve in Figure 2.

The accuracy of this calculation therefore depends only on the reliability of the assumption regarding the rectilinear fall of the propeller thrust and on the accuracy of the values calculated for the torque stand and for the take-off. This matter will receive more detailed attention farther on.

3. Minimum Ground Run - Effect of Wind

It is now easy, with formulas (3a) and (3b), to calculate also the shortest possible starting run. The ground run is the shortest when the force P assumes its maximum value at every instant. From the force diagram it follows that this condition is directly fulfilled on the resistance curve by the tangent from the point on the ordinate which represents the ground friction. The gain ΔP_m is inconsiderable in most cases. However, since the process of determining the maximum P_m is so simple, it is always advisable to use it.

This means that the airplane runs with the angle of attack corresponding to q_r. On reaching q_1 the pilot pulls up to the corresponding angle of attack and thus lifts the airplane from the ground. In Figure 3 it is obvious that the effect of this procedure is all the greater, the smaller the ground friction in comparison with the minimum air resistance, and the nearer q_1 approaches the minimum dynamic pressure. For a short ground run, q_1 is made as small as possible, but we will see later that the minimum total take-off distance is greatly affected by the transition arc and lies therefore at a somewhat greater q_1.

The effect of a head wind on the ground run is a double one. A head wind of v_w reduces the ground speed required for the lift-off to $v_1 - v_w$. At the same time the propeller efficiency is increased and the thrust correspondingly reduced. The latter effect is of a subordinate nature. In Figure 1 this is taken into account by choosing the dynamic pressure $q_w = \frac{\rho}{2} v_w^2$ as the initial dynamic pressure instead of the origin. A somewhat smaller value P_{m_w} is thus obtained for the mean accelerating force.

The reduction of the take-off speed can be expressed

directly in formula (3b). The ground run in a head wind then becomes

$$s_{1_W} = \frac{G}{P_{m_W}} \frac{(v_1 - v_W)^2}{2g} \tag{3d}$$

So long as v_W^2 remains small in comparison with v_1^2 (i.e., up to about $v_W/v_1 = 0.2$), the ground run in a head wind can be converted with sufficient accuracy to that in still air by the formula

$$s_1 = \frac{s_{1_W}}{1 - 2\frac{v_W}{v_1}} \tag{3e}$$

in which v_1 is the ground take-off speed (determined, e.g., by photographic measurement) plus the measured wind velocity v_W. In the region under consideration this is $P_m \approx P_{m_W}$.

It is obvious from (3d) that a weak head wind has a relatively great effect. A wind equal to 10 per cent of the take-off speed, e.g., reduces the ground run by about 20 per cent.

4. Transition to Climb

The total take-off distance up to a given altitude h consists of three phases (fig. 4): The ground run (s_1), the transition arc (s_2), and the climb (s_3). The known formulas disregard the transition arc, though the consequent error, as we shall see, is not always small.

After the lift-off, the pilot pulls on the control stick and forces the airplane into an upward curve. Despite the increased drag there is generally an excess momentum which carries the airplane along but, as the slope increases, this excess diminishes and may even become negative, so that the motion is retarded. On attaining the best slope for climbing, the pilot adjusts the elevator control in the corresponding position and continues to climb in a straight line.*

*Zooms, such as are often made in obstacle races, are disregarded here, since they have no commercial importance.

The problem is now to develop a general differential equation for this motion and then, by variation of the independent variables, to determine the best form of the transition arc. This problem is exceedingly complex, due to the interdependence of the variables (distance, dynamic pressure, air resistance). The difficulties in its solution would be entirely disproportionate to the importance and the requisite accuracy of the calculation. Hence only a simple approximation is here attempted.

First of all it is assumed that the airplane, after the take-off, describes an arc with the constant radius r, until it acquires the slope φ suitable for continuous climbing. For the moderate values of φ ($\cos\varphi \approx 1$) involved, we then have

$$s_2 = \varphi r \tag{4}$$

First arises the question regarding the ratio between the dynamic pressure and the lift coefficient at constant r. This is determined from the centripetal acceleration

$$\frac{v^2}{r} = g\left(\frac{A}{G} - 1\right)$$

Herefrom, with the known relations, we obtain

$$\frac{1}{r} = \frac{\gamma}{2}\left(\frac{c_a}{G/F} - \frac{1}{q}\right) \quad (= \text{const.}) \tag{5}$$

It is obvious that the lift coefficient at constant radius is inversely proportional to the dynamic pressure, i.e., the pilot must first pull up the elevator, then let it back a little and finally pull again stronger, in order to describe an arc. The radial acceleration then goes with the dynamic pressure, while the tangential acceleration depends on the path forces.

Expression (5) holds good for every part of the arc, e.g., the upper end. There expression (5) becomes

$$r = \frac{2}{\gamma}\frac{G}{F}\frac{1}{c_{a_2} - c_{a_3}},$$

since c_{a_2} is the lift coefficient at the end of s_2. The loss from the transition arc is proportional to r, which has its minimum value, when

$$c_{a_2} = c_{a_{max}}$$

Then
$$r = \frac{2}{\gamma}\frac{G}{F}\frac{1}{c_{a_{max}} - c_{a_3}} \qquad (6)$$

The value of c_{a_3} is first determined from the best condition for climbing. A smaller c_{a_3} may give a better total distance, however, since the loss in the transition arc is smaller.

The beginning of the arc will now be considered and the conditions at the beginning (c_{a_2}') and at the end ($c_{a_{max}}$) of the arc will be combined with each other according to formula (5).

$$\frac{c_{a_2}'}{G/F} - \frac{1}{q_1} = \frac{c_{a_{max}}}{G/F} - \frac{1}{q_3}$$

From this we obtain, by a simple transformation, the relation between the lift coefficients at a constant radius of the arc.

$$c_{a_{max}} - c_{a_2}' = c_{a_3} - c_{a_1} \qquad (7)$$

Here c_{a_1} and c_{a_2}' are still entirely optional. A minimum value of the ground run s_1 is obtained by (3c), when c_{a_1} is as great as possible. According to formula (7), however, we have

$$c_{a_1} \leqq c_{a_3},$$

since otherwise c_{a_2}' would be greater than $c_{a_{max}}$.* We would thus have the obvious result that the distance $s_1 + s_2$ would be the smallest when the beginning and end of the arc are flown at $c_{a_{max}}$. The middle portion, on the contrary would, according to formula (5), be somewhat smaller on account of the smaller c_a.

As to how far this is possible, depends on the force relations. Here it is very opportune that the polar is generally very flat at the maximum lift, so that it is almost always possible to fly in the vicinity of $c_{a_{max}}$ in such a way that the balance of the path forces is neutralized. Appreciable deviations can occur only with airplanes of exceptionally large or small excess power. In future

*The effect of the rate of change of the angle of attack on the maximum lift is disregarded.

we will therefore base our calculations on the following assumptions.

$$c_{a_1} = c_{a_3}, \text{ that is, } q_1 = q_3$$
$$c_{a_2} = c_{a_2}' = c_{a_{max}} \tag{8}$$

With respect to the simple geometric relation between the forces during the climb

$$\frac{P_1}{G} = \sin \varphi \approx \varphi,$$

equations (4) and (6) then become

$$\left.\begin{aligned} s_2' &= \frac{2}{\gamma} \frac{P_1}{F} \frac{1}{c_{a_{max}} - c_{a_1}} \\ \text{or} \qquad s_2 &= \frac{2}{\gamma} \frac{P_1}{G} \frac{q_1}{\frac{c_{a_{max}}}{c_{a_1}} - 1} \end{aligned}\right\} \tag{9}$$

It now follows from Figure 4 that the loss from the transition arc equals just half of the transition distance s_2, since the airplane is then climbing. We can make the calculation as if the airplane, immediately after leaving the ground, were climbing at the angle φ, if we add a lost distance

$$s_2' = \frac{P_1}{\gamma F} \frac{1}{c_{a_{max}} - c_{a_1}} = \frac{P_1}{\gamma G} \frac{q_1}{\frac{c_{a_{max}}}{c_{a_1}} - 1} \tag{10}$$

to the distances s_1 and s_3.

The climbing distance from the ground to the altitude h, according to Figure 4, then becomes

$$s_3' = \frac{h}{\tan \varphi} \approx \frac{h}{\sin \varphi} = h \frac{G}{P_1} \tag{11}$$

Formula (10) is also quite helpful in the designing of airplanes with respect to their take-off characteristics. The greatest effect on the distance s_2 is produced by the difference $c_{a_{max}} - c_{a_1}$. Slotted wings and similar devices for increasing the lift can increase this difference to a multiple of its normal value and thus make the transition

arc very short, as could recently be observed for the airplanes participating in the European circuit flight.*

IV. NONDIMENSIONAL THRUST DIAGRAMS

1. Bendemann's Limit

If it is desired to find a general law for the course of the propeller thrust, inquiries will first be made regarding the physical possibilities of the upper limit. It might indeed happen that the actual thrust curve would closely follow the theoretical limit in a way similar to the drag of a wing which differs from the induced drag only by an almost constant amount.

The relation between the thrust limit and the speed was indicated by Bendemann. (Reference 3.) In this connection he considers only the axial acceleration of the slipstream, where the additional speed and the thrust are considered uniformly distributed over the whole cross section of the slipstream. Further losses, which are occasioned on the actual propeller by rotation of the slipstream, finite blade number and profile drag, will be included later in a figure of merit. We obtain the relation between the "ideal" or limiting thrust S_{id} and the flight speed v through the transformation of the two well-known expressions

$$\eta_a = \frac{2}{1 + \sqrt{1 + c_s}}$$

$$c_s = \frac{S_{id}}{\frac{\rho}{2} v^2 F_s}$$

with consideration of the circumstance that

$$\eta_a = \frac{S_{id} V}{N}$$

Therefrom follows the limiting equation for the ideal thrust

$$S_{id}^3 + 2 \rho F_s N v S_{id} - 2 \rho F_s N^2 = 0 \qquad (12)$$

*For unlimited $c_{a_{max}}$ in the limiting case, we would have $r = 0$. This would correspond to a momentary deflection, such as might be caused by a guide rail with a notch.

as a function of the flight speed v, of the propeller-disk area F_s, of the engine power N, and of the air density ρ. For convenient evaluation, we will write equation (12) in the following form:

$$v = \frac{2 \rho F_s N^2 - S_{id}^3}{2 \rho F_s N S_{id}} \tag{13}$$

2. Nondimensional (S,v) Limiting Curve

Equation (13) can be easily made nondimensional. For greater clearness we introduce

$$(2 \rho F_s N^2)^{1/3} = S' \tag{14}$$

and then obtain the expression

$$v \frac{S'}{N} = \frac{1 - \left(\frac{S_{id}}{S'}\right)^3}{\frac{S_{id}}{S'}} \tag{15}$$

The left side of equation (15) is a nondimensional function of the speed; the right side, a nondimensional function of the thrust. In order to make the physical relation clearer, it is temporarily assumed that the power included in the propeller disk is independent of the speed. Then equation (14) is the well-kmown Bendemann expression for the limiting thrust on the torque stand (S_{id}/S'), that is, the ratio of the limiting thrust at the speed v to the limiting thrust on the torque stand. The thrust function drops from 1 to 0 when the speed function increases from 0 to ∞. (Fig. 5.)

When N is constant, the abscissa represents the speed and the ordinate the ideal thrust. If, on the contrary, N depends on v, then the two axes no longer strictly represent this simple relation. We will see later, however, that N is generally sufficiently constant in the range of operation of actual propellers.

3. Introduction of Experimental Values

Moreover, the experimental values of actual propellers can be introduced into this scheme. It is only necessary to substitute the experimental thrust S for the limiting thrust S_{id}. The two coordinates then receive the following designations.

$$\left.\begin{aligned} v\,\frac{S'}{N} &= v\,\frac{(2\,\rho\,F_s\,N^2)^{1/3}}{N} = v\left(2\,\rho\,\frac{F_s}{N}\right)^{1/3} &&= \Phi \\ \frac{S}{S'} &= \frac{S}{(2\,\rho\,F_s\,N^2)^{1/3}} &&= \Sigma \end{aligned}\right\} \qquad (16)$$

It would be very inconvenient, however, to calculate the speed coefficient Φ and the thrust coefficient Σ with these formulas. Hence we introduce the coefficients k_s, k_d, and η into formula (11) and obtain

$$\left.\begin{aligned} \Phi &= \lambda\left(\frac{4}{k_d}\right)^{1/3} = \left(\frac{4}{c_l}\right)^{1/3} \\ \Sigma &= \frac{k_s}{(2\,k_d)^{2/3}} = \eta\left(\frac{c_l}{4}\right)^{1/3} \end{aligned}\right\} \qquad (17)$$

The abscissa therefore behaves like the reciprocal of the third root of the performance factor c_l, while the ordinate is of the form $c_a/c_w^{2/3}$ and therefore corresponds to the well-known coefficient of climb.

The experimental values can be very easily transformed by calculation with formulas (17) for our diagram. For further facilitation the corresponding formulas for the evaluation of the American N.A.C.A. experiments are given

$$\left.\begin{aligned} \Phi &= 1.16\,\frac{v}{n\,D}\,C_p^{1/3} \\ \Sigma &= 0.86\,C_T/C_p^{2/3} \end{aligned}\right\} \qquad (17a)$$

An example is given in Figure 6. The axial efficiency η_a is plotted as the product of Σ_{id} and the corresponding Φ. Moreover $\Phi\,\Sigma = \eta$ holds good for every point of the field according to formulas (17).

Lines of constant efficiency (η_{free}) are plotted. These show the efficiency it is possible to attain with the individual propellers. The quality of the propellers under given conditions of operation is measured by the degree of approximation to the limiting thrust. A criterion for this is the Bendemann figure of merit.

$$\zeta = \frac{S}{S_{id}} = \frac{\Sigma}{\Sigma_{id}} \tag{18}$$

Air propellers can thus be compared and evaluated. In the most different propellers (of course, only good ones), ζ is found to be remarkably constant. In the most important range of operation, it has a value of 0.88 to 0.89. It grows worse, however, on approaching the condition $\Phi \rightarrow 0$. For this reason it is not possible in take-off calculations to use the curve of the ideal thrust as the basis of an approximation.

4. Revolution Speed and Engine Power

If it is at first assumed that the engine power is constant, i.e., independent of the revolution speed, then the latter (n), according to the universal law of similitude (M. Schrenk, loc. cit.) for otherwise given dimensions, is proportional to the third root of the effective torque k_d. The revolution speed for every propeller and every operating condition can thus be easily determined from the corresponding k_d curve. If the engine power is a function of the revolution speed, it was shown by M. Schrenk that two approximations for the n,N curve make it possible to determine satisfactorily the relations in the whole practical range, namely,

$$N \sim n^{1/2} \qquad N \sim n$$

With the aid of the law of similitude, these values can be easily introduced into formulas (16) by substituting for the variable engine power a constant value, which is defined by a definite operating condition, e.g., the torque stand. For the law of the roots we then have

$$\left.\begin{aligned} \Phi &= v\left(2\,\rho\,\frac{F_s}{N_o}\,\frac{N_o}{N}\right)^{1/3} = v\left(2\,\rho\,\frac{F_s}{N_o}\right)^{1/3}\left(\frac{k_d}{k_{d_o}}\right)^{1/15} \\ \Sigma &= \frac{S}{\left(2\,\rho\,F_s\,N_o^{\,2}\left(\frac{N}{N_o}\right)^2\right)^{1/3}} = \frac{S}{(2\,\rho\,F_s\,N_o^{\,2})^{1/3}}\left(\frac{k_d}{k_{d_o}}\right)^{2/15} \end{aligned}\right\} \tag{19a}$$

If it is now considered that, according to Figures 8-10, the effective torque k_d generally varies in the practically important region by only ±20 to 25 per cent, the effect of the variation in the effective torque on formulas (19a) is then so small that it can be disregarded for practical purposes.

If, on the contrary, the engine power follows the revolution speed (constant torque)* the coordinates become

$$\left.\begin{aligned} \Phi &= v\left(2\,\rho\,\frac{F_s}{N_o}\,\frac{N_o}{N}\right)^{1/3} = v\left(2\,\rho\,\frac{F_s}{N_o}\right)^{1/3}\left(\frac{k_d}{k_{d_o}}\right)^{1/3} \\ \Sigma &= \frac{S}{\left(2\,\rho\,F_s\,N_o^2\left(\frac{N}{N_o}\right)^2\right)^{1/3}} = \frac{S}{(2\,\rho\,F_s\,N_o^2)^{1/3}}\left(\frac{k_d}{k_{d_o}}\right)^{1/3} \end{aligned}\right\} \quad (19b)$$

In this case, for any fairly accurate calculation, the effect of the revolution speed on the output can no longer be disregarded. The velocity coefficient and thrust coefficient of Figure 6 no longer represent any linear function of the velocity and thrust, which is inconvenient for flight calculations. This situation can be improved by introducing new velocity and thrust coefficients through division by the corresponding k_d functions.

$$\left.\begin{aligned} \Phi' &= \frac{\Phi}{(k_d/k_{d_o})^{1/3}} = \frac{(4/k_d)^{1/3}}{(k_d/k_{d_o})^{1/3}} = v\left(2\,\rho\,\frac{F_s}{N_o}\right)^{1/3} \\ \Sigma' &= \frac{\Sigma}{(k_d/k_{d_o})^{1/3}} = \frac{k_s/(2k_d)^{2/3}}{(k_d/k_{d_o})^{1/3}} = \frac{S}{(2\,\rho\,F_s\,N_o^2)^{1/3}} \end{aligned}\right\} \quad (20)$$

*This is the assumption in the treatise on variable-pitch propellers published by Reissner and Schiller in the 256th D.V.L. Report (Z.F.M., Vol. 22, 1931, No. 18, pp. 551-557, and D.V.L. Yearbook, 1932). There the nondimensional coefficients $(1/c_s)^{1/2}$ (with a constant factor) and k_s/k_d are used. For the purpose of that representation, there was to be followed, above all, the effect of the variation of the propeller pitch on the thrust at constant torque, variable speed, and at any revolution speed (preferably constant).

With Φ' and Σ' the coordinates of the general thrust diagram (fig. 5) at constant engine torque again receive the signification of velocity and thrust. The reference power N_o is the engine power at the torque-stand r.p.m. of the propeller.

Graphs of this kind are practical when there is much calculation to be made with engines of constant torque. They are not necessary, however, for take-off calculations, since allowance can easily be made for the variation of k_d in this region by adopting a mean engine output.

V. STATIC THRUST

1. Lack of Experimental Results

The N.A.C.A. data used in this treatise (there being no German data available) lack in one particular; the static thrust is nowhere given. This is probably due to the fact that the torque-stand conditions can never be obtained in a wind tunnel with circulation, since, with the blower stopped, the propeller generates its own relative wind. In future tests the results should be supplemented by a measurement of the static thrust with the same propeller and arrangement, but outside the wind tunnel.

The British data (reference 4), which are not included in this report but which have also been investigated, are distinguished by a systematic choice of propellers and also include the static thrust. Nevertheless, due to their unbelievably high figure of merit (ζ_o up to 90 per cent), these static-thrust data cannot be used, because they were apparently obtained in a closed wind tunnel. From Figure 7 it is obvious that the inflow to the propeller is completely changed by the walls of the tunnel.

The flow conditions on the torque stand were largely determined by the experiments of Bendemann and Schmidt. (Reference 5.) Glauert and Lock arranged the results of their investigations, as established for the point $\lambda = 0$, in a comprehensive picture of the course of the flow at any positive and negative coefficient of advance and thrust. (Reference 6.) From this it follows that, for propellers which work at a small positive or negative coefficient of advance, the air flows in from all sides

with the formation of a sort of vortex ring. It is the lateral inflow which has hitherto resisted all attempts to develop a rational theory of the propeller on the torque stand. Probably it is also responsible for the previously mentioned decrease in the figure of merit, even in cases where the angle of attack of the blade is still below the critical point with respect to the inflow, and therefore the flow past the blade has probably not yet become detached. If this inflow from all sides is prevented by conducting the air between walls, the flow picture is smoothed out, thus correspondingly increasing the figure of merit.

2. Quadratic Extrapolation

There is therefore nothing else to do but to extrapolate the static thrust from the American data. In order to proceed systematically, it was assumed that the thrust coefficient is parabolic in the vicinity of zero coefficient of advance. This assumption was also warranted by the use to be made of it.

In order to facilitate the parabolic extrapolation, the test values were plotted against the square of the coefficient of advance. (Figs. 8-10.) The small piece between the last test point and the zero coefficient of advance was rectilinearly extended for the thrust coefficient. For the effective torque, on the contrary, the curves were extrapolated according to their general course. Naturally such a method may raise certain doubts. It appears, however, to be accurate enough for the purpose* and yields, moreover, too low rather than too high static-thrust values, thus affecting the calculation on the safe side. Of course it would be better if measured static-thrust data were available.

3. Static-Thrust Figure of Merit

From these test results the static-thrust figure of merit

---

*From the fact that, for the calculation of the ground run, it is integrated over q, it follows that the condition in the vicinity of $v = 0$ does not matter much.

$$\zeta_0 = \frac{k_{s_0}}{(2\,k_{d_0})^{2/3}} = 0.86\frac{c_{T_0}}{c_{P_0}{}^{2/3}} \qquad (21)$$

can now be calculated. Since, according to Section III, the static thrust is necessary for the take-off calculation, the static-thrust figures of merit must be specially determined, in order to provide a basis for the approximate calculation. Lacking a rational theory of the static thrust, which would determine the effect of the propeller shape, one is left in doubt as to what parameter the static-thrust figure of merit should be plotted against. It can be safely said only that the flow will separate at too high a blade angle. Since the blade angle, however, depends on the pitch ratio H/D, this should be chosen as an independent variable. Thus we obtain Figure 11, in which a broken line interpolates the ζ_0 values measured on three series of propellers.

The resulting static-thrust figure of merit of 0.74 in the most favorable region is considerably lower than what is customarily assumed. The comparison of the ground runs calculated with these low values with the measured runs, makes it probable, however, that the low values are correct.

Under the corresponding assumption that ζ_0 is probably constant in the customary region (with otherwise like execution) we have, according to equation (16),

$$S_0 \sim F_s{}^{1/3} \sim D^{2/3}$$

This shows how much can be gained in the static thrust by increasing the diameter, whereby large diameter variations naturally necessitate corresponding variations in the revolution speed, for the propeller to remain in the best working range.

VI. FLIGHT RELATIONS

1. Thrust and Drag against the Dynamic Pressure

Since the take-off formulas in Section III are based on the dynamic pressure, it is also logical to plot the nondimensional thrust curve against the dynamic pressure. For this purpose, Φ is simply squared according to formu-

las (16) and (17), giving

$$\Phi^2 = q\left(\frac{32}{\rho}\right)^{1/3}\left(\frac{F_s}{N}\right)^{2/3} = \lambda^2\left(\frac{4}{k_d}\right)^{2/3} = \left(\frac{4}{c_l}\right)^{2/3} = \theta \qquad (22)$$

Figures 12 and 13 were plotted with this abscissa. Of course the Bendemann limit also occurs here.

It is now necessary to introduce into this representation the drag of the given airplane in addition to the theoretical calculations. This method seems more practical than that of plotting the thrust curves in a drag diagram since, in the first case, it is necessary to calculate and plot only a single curve but, in the other case, a whole group.

Moreover, the drag curve in normal flight is very easy to plot, if it is remembered that, according to known relations (with c_{w_p} and c_{w_r} as constants), it is composed of a straight line through the origin (head resistance) and an equilateral hyperbola (induced drag), which latter can be easily constructed with a few subsidiary lines. The deviations of the actual resistance curve from this ideal curve need to be considered only in the region of high lift coefficients (below θ_c).

The drag of an airplane is therefore based on the approximate quantity S' (equation 14) corresponding to the ideal static thrust, and the new nondimensional value is then obtained for the drag

$$\Psi = \frac{W}{(2\ \rho\ F_s\ N^2)^{1/3}} \qquad (23)$$

The drag coefficient Ψ corresponds perfectly to Σ in its application in the force diagram. If, for example, we have F_{w_s} and W_{min} $(= \epsilon_{min}\ G)$, then F_{w_s} = constant means a definite line through the origin. (More about this in the next section.) W_{min} = constant is a parallel to the abscissa at the distance

$$\Psi_{min} = \frac{W_{min}}{(2\ \rho\ F_s\ N^2)^{1/3}}$$

At the point of best lift-drag ratio the head resistance is just half of the total drag. From this we obtain

θ_ϵ and q_ϵ. Moreover the whole drag curve can be plotted as a hyperbola according to known methods (Hütte I).

2. Drag Increase in Slipstream

Thus far the procedure has been as though the propeller and airplane were working independently of each other. In reality the velocity field of the airplane disturbs the slipstream, and the latter increases the drag of the airplane.

Generally this phenomenon is summarily accounted for by deducting ΔW from the propeller thrust, which is expressed by the disturbance factor η_s as follows:

$$S - \Delta W = \eta_s S \tag{24}$$

We will calculate in a practical manner, as though only the quantity $\eta_s S'$ were present instead of the reference quantity S'. (Equation 14.) From our diagram we then obtain

$$\left.\begin{aligned} S &= \Sigma \eta_s S' \\ W &= \Psi \eta_s S' \end{aligned}\right\} \tag{25}$$

We must bear in mind that, according to equation (25) with the introduction of $\Psi = W/\eta_s S'$ the drag curve is increased by the factor $1/\eta_s$, while the thrust curves remain unaltered. This may seem confusing at first thought, but is no more than a change in the scale to save work in plotting.

3. Propeller-Blade Ratio and Load Factor

Moreover, with the aid of equations (22) and (25), we can write

$$\frac{\Psi}{\theta} = \frac{W}{4\ q\ \eta_s\ F_s} = \frac{S}{4\ q\ F_s} = \frac{c_s}{4}$$

for the lines through the origin. After the transposition with $W/q = F_w$ we have

$$\eta_s \frac{F_s}{F_w} = 0.25\ \frac{\theta}{\Psi}$$

Since ψ and Σ may be exchanged in the diagram, we obtain, with equations (17) and (22),

$$0.25 \frac{\theta}{\psi} = 0.25 \frac{\theta}{\Sigma} = \eta_s \frac{F_s}{F_w} = \frac{1}{c_s} \qquad (26)$$

Lines through the origin ($\frac{F_s}{F_w}$ = constant) are therefore lines of constant load factor. The load factor depends (aside from the disturbance factor η_s) only on the area ratio F_s/F_w.

If the lines for constant F_s/F_{w_s} are now drawn (figs. 11 and 12), they immediately give a picture of the load factor at every point of the field. The load factor determines the maximum efficiency.

In the quantity F_s/F_{w_s} we find an old acquaintance, namely, the propeller-blade ratio. It was previously found that this ratio determined the load factor for the best lift-drag ratio. It was

$$c_{s_\epsilon} = \frac{2}{\eta_s} \frac{F_{w_s}}{F_s}$$

When it is recalled that $F_{w_s} = \frac{1}{2} F_{w_\epsilon}$, the identity of this expression with equation (26) is confirmed. Only equation (26) is much more general and holds good for any operation point.

In Figure 14 these relations are illustrated by an example. The drag curve is determined by

$$\psi_{min} = 0.25$$

and

$$\eta_s \frac{F_s}{F_{w_s}} = 4$$

from which follows $\theta_\epsilon = 2$

The drag curve is plotted as a hyperbola between ordinates and the given line by $\eta_s \frac{F_s}{F_{w_s}} = 4$. Below θ_ϵ a mean curve is added under consideration of the separation phenomenon. Three propeller curves are plotted for choosing from. The choice of the right propeller depends on the use and also on the revolution speed.

4. Thrust Curves

Since the load factor, efficiency and coefficient of advance are constant along the line through the origin, such a group of lines can be easily used for plotting the thrust curves, similarly to the method previously followed in the (N,v) diagram with the aid of the thrust parabola. Here the relationship between thrust, engine power and air density must be taken into consideration, which, in correspondence with the formula for the static thrust, then becomes

$$S \sim (\rho N^2)^{1/3} \sim \rho^{1/3} N^{2/3} \qquad (27)$$

If therefore the engine output is reduced 50 per cent, e.g., the thrust drops, for the same coefficient of advance, to $0.5^{2/3} = 0.63$ of the original. All the ordinates along the lines through the origin are now shortened, in order to obtain the points for the thrust curve at 50 per cent engine output.

Since the present work chiefly concerns the take-off, we will not carry this line of thought further, nor illustrate it by diagrams.

VII. PRACTICAL EXAMPLE

The above deductions and statements will now be illustrated by an example. For this purpose we have chosen a German sport biplane whose aerodynamic characteristics were derived from flight-performance data in the previously mentioned work by the writer. The total take-off distance up to a flight altitude of 20 m (about 66 feet) will be calculated. The data for the airplane are as follows:

N_o =	330 hp	F_{w_s} =	1.45 m^2
G =	1835 kg	b_i =	13.6 m
F =	36.7 m^2	ϵ_{min} =	1/10 (= $f(b_i, F_{w_s})$)
D =	3 m	η_s =	0.85

From these values we obtain

$$q_\epsilon = 63 \text{ kg/m}^2 \quad \text{and} \quad ca_\epsilon = 0.80$$

for the flight condition of best lift-drag ratio with a wing loading of about 50 kg/m² (10.24 lb./sq.ft.). For plotting in the nondimensional propeller-thrust diagram, the fundamental value of the ordinates must first be determined from equation (25).

$$\eta_s S' = 0.85 \times 1025 = 870 \text{ kg}$$

In the calculation of S' we assume that $N = N_o$, since the effect of the variation in the revolution speed in taking off is small. Here the ordinate of the minimum drag is

$$\Psi_{min} = \frac{W_{min}}{\eta_s S'} = \frac{0.1 \times 1835}{870} = 0.21$$

The second place for the drag hyperbola is the line through the ordinate with

$$\eta_s \frac{F_s}{F_{w_s}} = 4.15$$

The intersection of these two lines yields

$$\theta_\epsilon = 1.74$$

Now the drag curve is plotted (fig. 15) to the right of θ_ϵ as a hyperbola, and to the left with a rounding up to contact with the vertical line corresponding to $c_{a_{max}} = 1.3$, whose abscissa should be θ_{min} (the airplane in question having a profile with a fixed center of pressure). On the basis of this complete thrust diagram, we must first select a particular propeller. Of the three metal propellers plotted, only the one with the 20.4° adjustment,* according to the conditions, comes into the question, since the take-off thrust rapidly decreases with increasing blade angle. This propeller will serve as the basis for our further consideration.

Formulas (3), (10), and (11) show a very diversified dependence on the determinative quantities P_m, P_1, and c_{a_1}. For the explanation, especially of the effect of

---

*And also an adjustment in its vicinity, whereby the diameter and revolution speed must be taken into consideration. (Section IV, 4.)

the transition arc (s_2), the take-off distance will therefore be calculated for various lift coefficients, whose minimum value (0.8) corresponds to c_{min}. After introducing the numerical values, the corresponding formulas read

$$s_1 = \frac{73000}{c_{a_1} P_m}$$

$$s_2' = \frac{1}{46} \frac{P_1}{c_{a_{max}} - c_{a_1}}$$

$$s_3' = \frac{36700}{P_1}$$

In the calculation it is advisable to introduce, in place of the P values, the nondimensional coefficients $\pi = \frac{P}{\eta_s S \gamma}$, which can be taken directly from the thrust diagram. Before measuring π_m the portion of the thrust curve between 0 and θ_1 is represented by a straight line by eye measurement. The ground-friction coefficient μ was assumed to be 0.075.

Figure 16 shows the result of the calculation plotted against the lift coefficient. It is obvious that the transition arc plays an important role only with lift coefficients in the vicinity of $c_{a_{max}}$. Nevertheless, the numerical value of the transition arc can no longer be disregarded in the best total distance. Here it is about 30 m (98 ft.). The error from using approximation formula (3) for the ground run is small in comparison, being 3 m (10 ft.) at the most.

With the exacted restraint, the conclusion can be drawn from the example that the best total take-off distance is obtained when the airplane is lifted off the ground by the dynamic pressure of steepest climb (maximum climbing power) and then, after the shortest possible and yet uniform transition, is brought to a steady climb with the same dynamic pressure.*

Attention is also called to the fact that no such good agreement between calculation and experiment can be

---

*This is moreover a long-known rule among test pilots.

expected in the take-off distance as in other flight performances notwithstanding the greatest care in the calculation. Inaccuracies in the assumptions (especially the effect of the slipstream on the drag and lift, and the ground effect (reference 7), and the peculiarities of the individual pilots may cause considerable discrepancies. With this reservation the test results obtained by the D.V.L. with the calculated specimen are:

Ground run,	170 m (558 ft.)
Total take-off distance,	525 m (1,722 ft.)

The ground run agrees satisfactorily with the calculated distance. On the contrary, the discrepancy in the climb is striking. It is presumable that the pilot took no pains to keep this distance as short as possible. The discrepancy may be very great, especially in the transition stretch, when flown at too small a coefficient of lift.

VIII. SUMMARY

The take-off consists of three parts: ground run, transition arc and climb to a given altitude, all three parts being taken together and calculated as a unit. The flight condition for the minimum ground run is obtained directly from the force diagram. A special consideration shows that the shortest total distance is obtained, when the lift-off is made with the lift coefficient of the climb and the transition arc is flown with the maximum lift. Under the conditions the total take-off distance s is calculated from the formula

$$s = \frac{G}{P_m} \frac{G}{\gamma F} \frac{1}{c_{a_1}} + \frac{P_1}{\gamma F} \frac{1}{c_{a_{max}} - c_{a_1}} + h \frac{G}{P_1}$$

The importance of the individual airplane characteristics (weight, accelerating force, wing area and lift coefficient) for the take-off distance proceeds directly from this extremely simplified formula. The ground run is the product of the take-off speed and the ratio of the accelerating force to the weight. The effect of the wind during the ground run is nearly proportional to the square of the air speed. The importance of the transition arc increases with the climbing power and decreases as the excess lift increases.

For calculating the accelerating force P_m and the climbing power P_1, a new nondimensional thrust-pressure diagram is developed, containing a theoretical upper limit for the thrust which greatly facilitates the search for the best propeller. In this connection the static thrust is more carefully considered. The Aleyrac assumption of a rectilinear course of the propeller thrust with respect to the dynamic pressure can be retained, since the actual thrust curve in the take-off region (but only in this region) can be closely approximated by a straight line. The static-thrust figures of merit to be introduced in this connection are considerably lower than the customary values. It is further shown how the drag curve easily conforms to this form of presentation. In this connection remarkable theoretical conclusions were reached, which, however, could only be considered briefly.

Lastly it is shown by means of a numerical example that the best lift coefficient for the take-off and climb are about the same as for the steepest climb. At still higher lift coefficients the effect of the transition arc is preponderant. Such high lift coefficients do not, however, come into the question on account of the danger involved, so that it may be said that the minimum practical take-off speed generally yields the shortest take-off distance, if flown steadily.

Beyond the scope of this paper, the work indicates ways to a general force diagram, which makes it possible to get a clear conception of all the phenomena of throttled and of unthrottled flight.

Translation by Dwight M. Miner,
National Advisory Committee
for Aeronautics.

REFERENCES

1. Blenk, H.: Startformeln für Landflugzeuge. Z.F.M., Vol. 18, No. 2, 1927, pp. 25-32; D.V.L. Yearbook, 1927, pp. 1-8.

2. Schrenk, M.: The Mutual Action of Airplane Body and Power Plant. T.M. No. 665, N.A.C.A., 1932.

3. Bendemann, F.: Wirkungsgrad und Gütegrad von Luftschrauben. Z.F.M., Vol. 9, No. 2, 1918, pp. 35-39.

4. Fage, A., Lock, C. N. H., Howard, R. G., and Bateman, H.: Experiments with a Family of Airscrews Including the Effect of Tractor and Pusher Bodies. Part I. Experiments with the Family of Airscrews Mounted in Front of a Small Body. R.& M. No. 829, British A.R.C., 1922.

5. Bendemann, F.: Der Strömungsvorgang an der Luftschraube im Stand. Z.F.M., Vol. 9, No. 1, 1918, p. 1.

6. Lock, C. N. H., Bateman, H., and Townend, H. C. H.: An Extension of the Vortex Theory of Airscrews with Applications to Airscrews of Small Pitch, Including Experimental Results. R.& M. No. 1014, British A.R.C., 1926.

   Glauert, H.: The Analysis of Experimental Results in the Windmill Brake and Vortex Ring States of an Airscrew. R.& M. No. 1026, British A.R.C., 1926.

7. Tonnies, E.: Effect of the Ground on an Airplane Flying Close to It. T.M. No. 674, N.A.C.A., 1932.

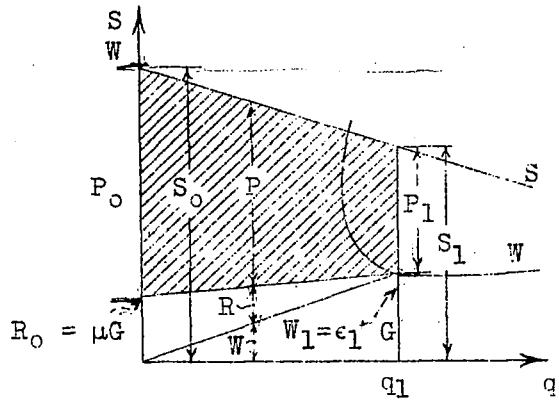

Figure 1.-Force diagram for take-off. In order to develop the formula for the ground run, the forces are plotted against the dynamic pressure. Ground friction and air resistance are deducted before integration. The accelerating forces determinative for the take-off lie in the hatched area.

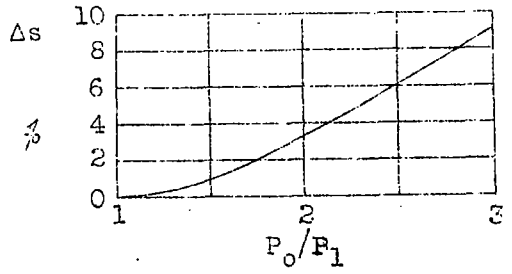

Figure 2.-Correction for formula 3. P_o/P_1 lies mostly under 2.

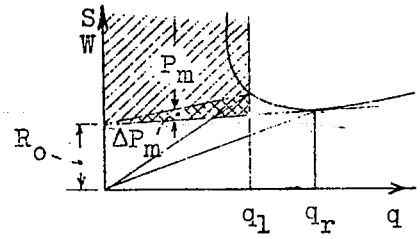

Figure 3.-For calculating the minimum ground run. The maximum accelerating forces and consequently the minimum ground run is obtained by a tangent of R_o on the drag curve. The cross-hatched area or ΔP_m represents the thus-obtained increase in the accelerating force.

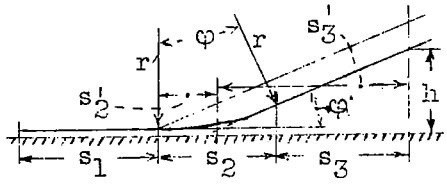

Figure 4.-For calculating the transition arc. The transition is assumed to be the arc of a circle. The loss from the transition arc is represented by a subsidiary distance s'_2 which corresponds to a climbing distance of s'_3.

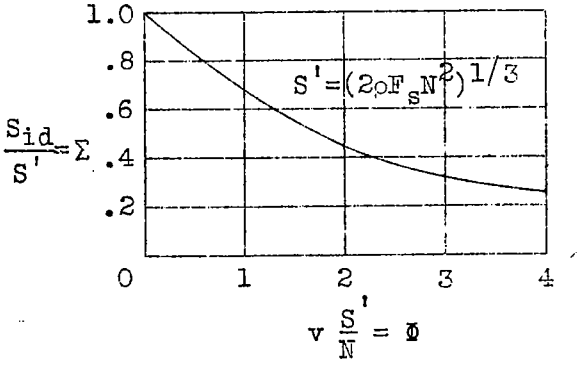

Figure 5.-Bendemann limiting curve for thrust in nondimensional representation. S' corresponds, in the use of engine power on torque stand, to the Bendemann ideal static thrust.

$$\Sigma = \frac{S}{(2\rho F_3 V^2)^{1/3}} = \frac{k_s}{(2k_d)^{2/3}} = \eta\left(\frac{c_l}{4}\right)^{1/3}$$

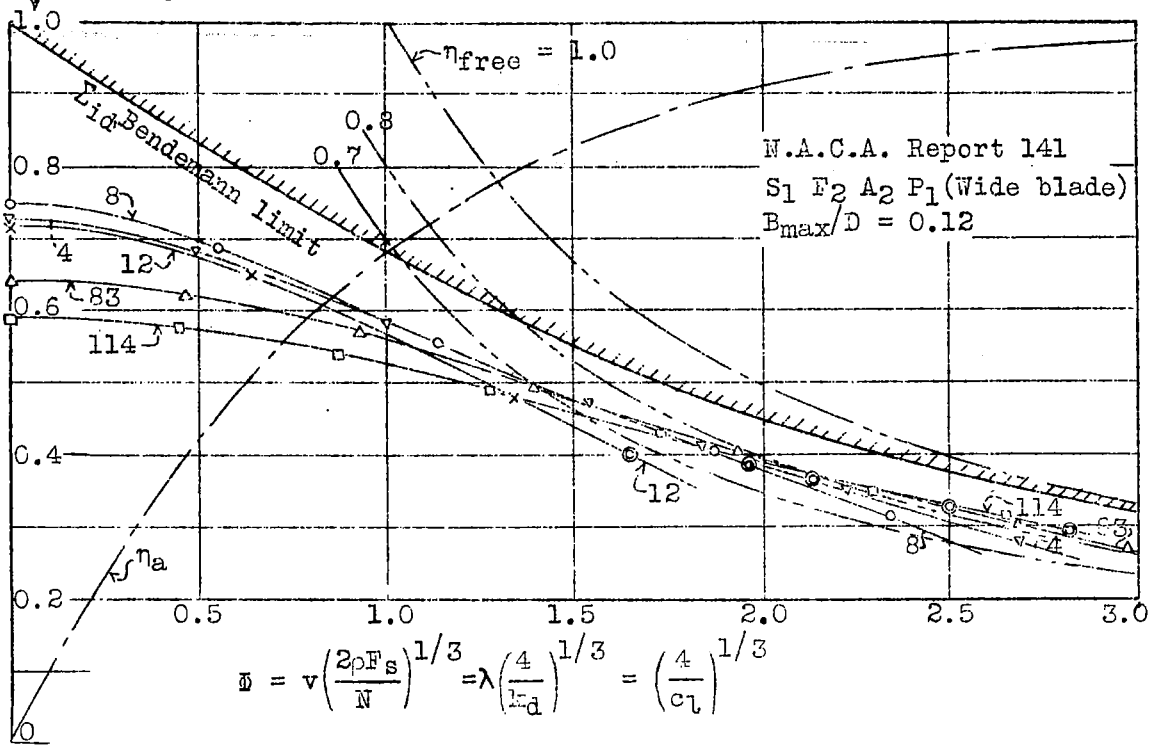

Propeller	12	8	4	83	114
H/D =	0.5	0.7	0.9	1.1	1.3
k_{d_o} =	0.0039	0.0061	0.0082	0.0100	0.0114

◎ Points of maximum efficiency

Figure 6.-Nondimensional graph of thrust over speed. The graph contains an American series of propeller tests, in which the propellers had different pitches. The distance of the curves from the Bendemann limit denotes the figure of merit of the propellers at the given point. Hyperbolas for constant efficiency η_{free}, as well as the curve for the axial efficiency η_a are also plotted.

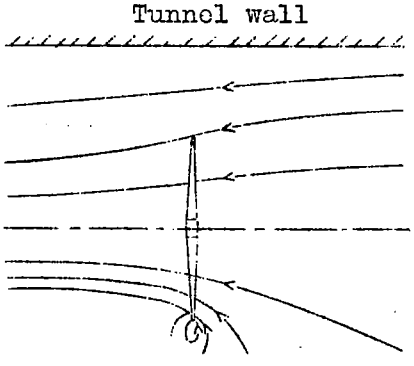

Figure 7.-Idealized streamline diagram of propeller on torque stand. The lower half represents the conditions with inflow from all sides; the upper half, the flow in a closed tunnel. It shows how the flow in the latter case is smoothed out by the effect of the tunnel walls, whereby the static thrust is naturally greater than in an unconfined air current.

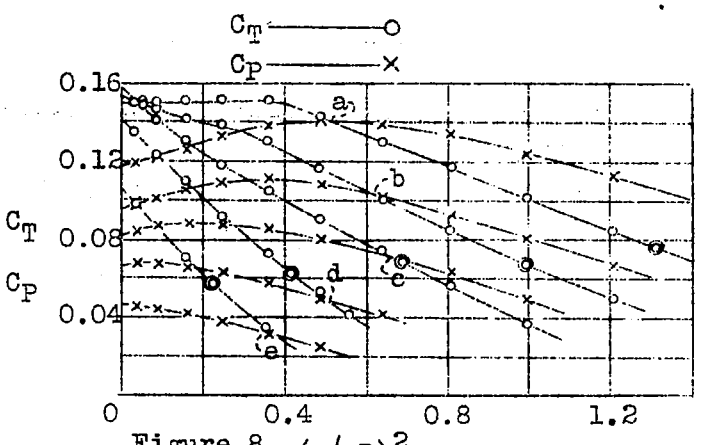

Figure 8. $(v/nD)^2$

C_T ——○
C_P ——×
a, Propeller 113, H/D=1.3
b, " 82 " =1.1
c, " 3 " =1.9
d, " 7 " =1.7
e, " 11 " =1.5

Report 141
$S_1 F_2 A_1 P_1$

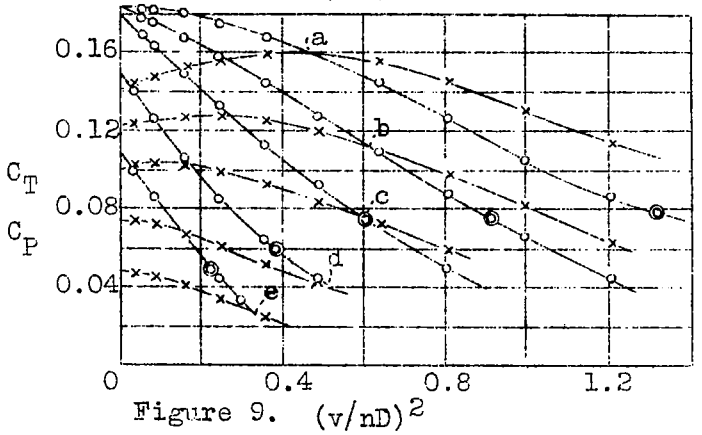

Figure 9. $(v/nD)^2$

C_T ——○
C_P ——×
a, Propeller 114, H/D=1.3
b, " 83 " =1.1
c, " 4 " =0.9
d, " 8 " =0.7
e, " 12 " =0.5

Report 141
$S_1 F_2 A_2 P_1$

Figures.8,9,10.-Coefficients for 3 propellers series plotted against the square of the coefficient of advance. The plotting is done in this way for the purpose of parabolic extrapolation of the thrust coefficient C_T.

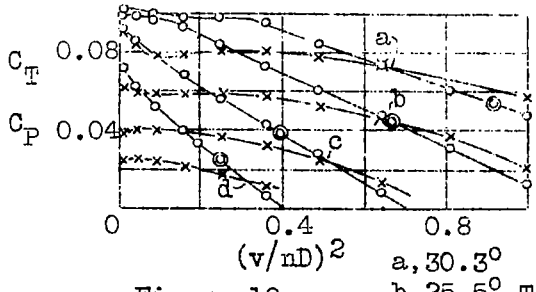

Figure 10.

a, 30.3°
b, 25.5°
c, 20.4°
d, 14.8°

T.N. 333 Variable-pitch propeller.

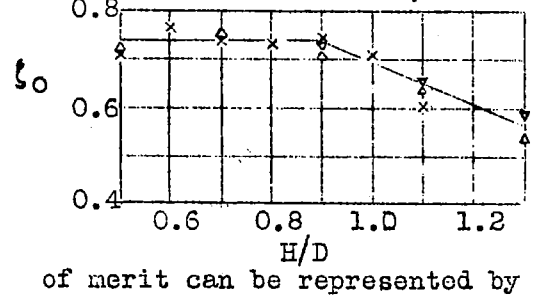

C_T ——○
C_P ——×

△ $S_1 F_2 A_1 P_1$ Report 141
▽ $S_1 F_2 A_2 P_1$
× Navy propellers, Report 237

Figure 11.-Static-thrust figures of merit for 3 series of wood propellers. The figures of merit can be represented by a broken line with sufficient accuracy for the design.

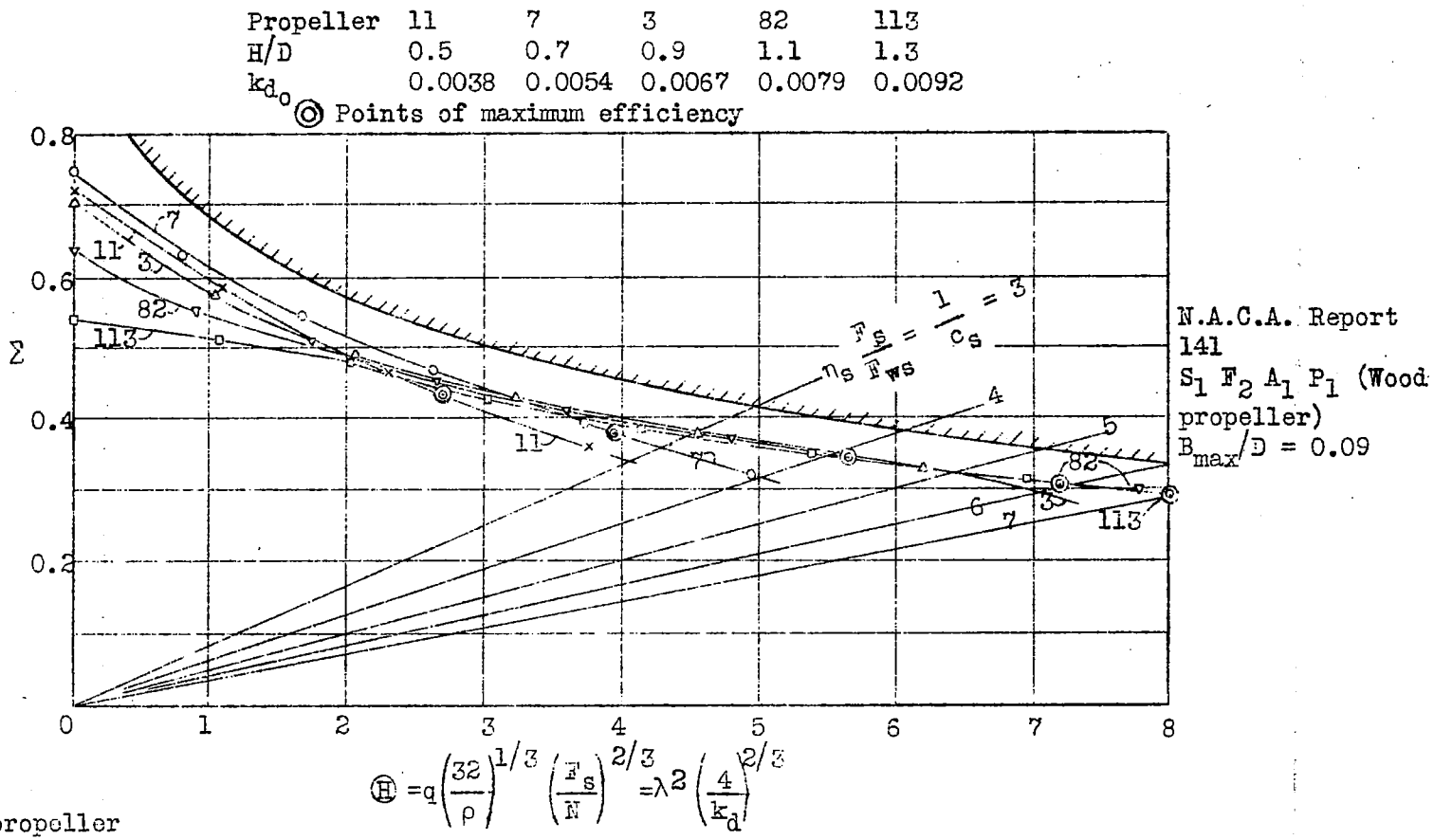

Wood propeller

Figure 12.-Nondimensional graphs of thrust over dynamic pressure. In the take-off region the thrust curves can be easily replaced by straight lines. The differences in the static thrust between the wooden propeller and the metal propeller are noteworthy. Lines of constant load factor are also plotted through the origin.

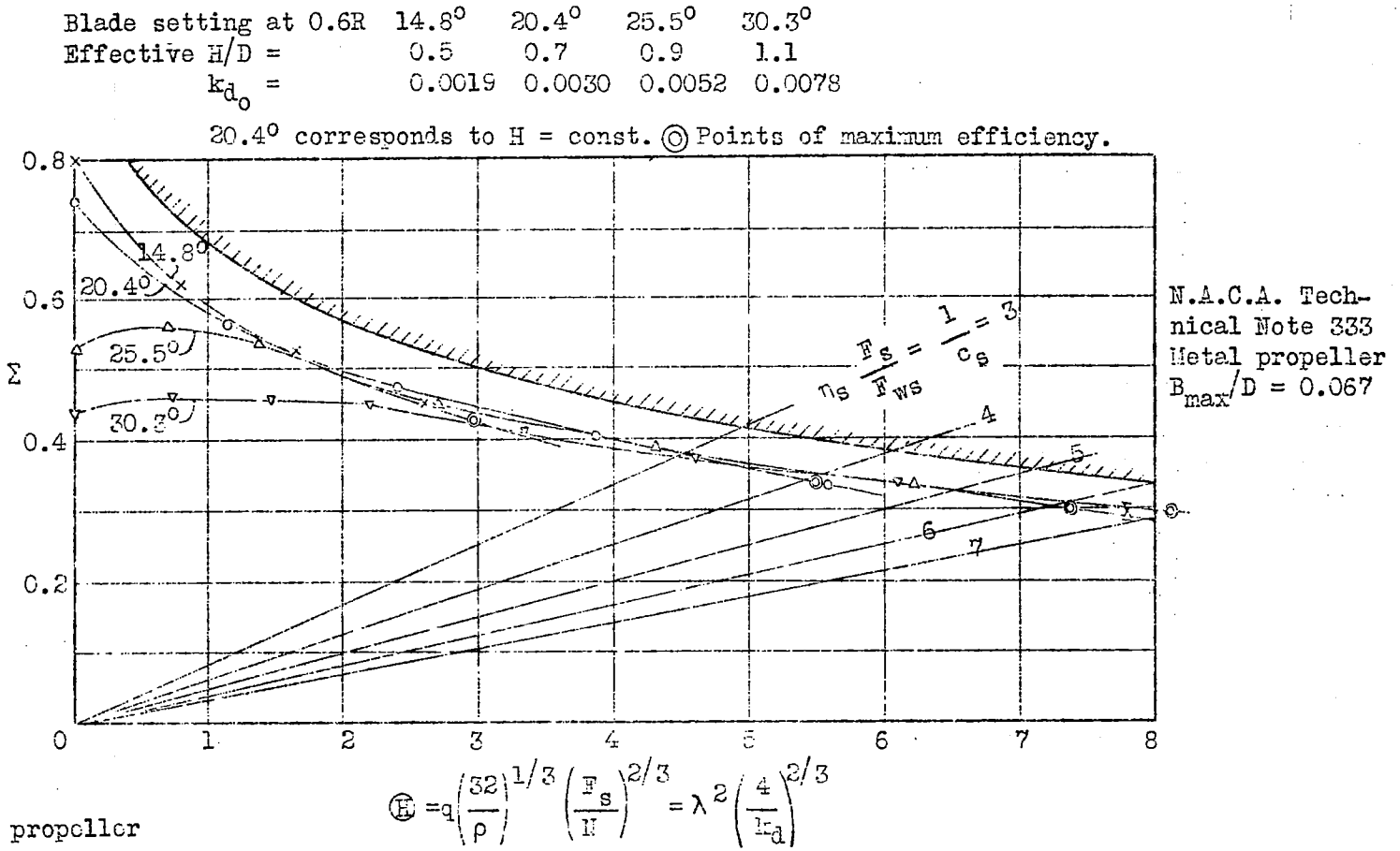

Figure 13.-Nondimensional graphs of thrust over dynamic pressure. In the take-off region the thrust curves can be easily replaced by straight lines. The differences in the static thrust between the wooden propeller and the metal propeller are noteworthy. Lines of constant load factor are also plotted through the origin.

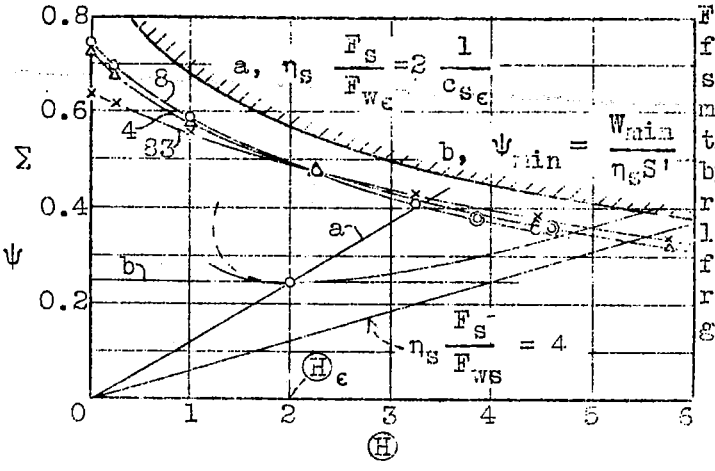

Figure 14.-Comprehensive force diagram. The air-resistance curve is determined by the ordinate of the minimum resistance and by the straight line which represents the asymptotic load factor. The load factor for the best L/D ratio is just twice as great.

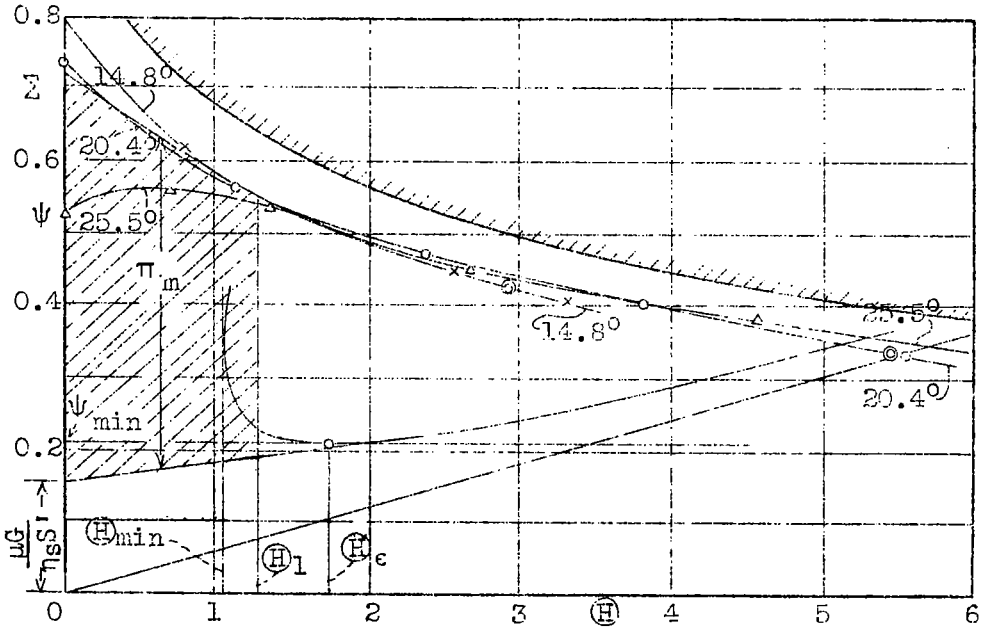

Figure 15.-Thrust and resistance curves for the example. The hatched area again determines the ground run. In it the propeller-thrust curve is represented by a straight line.

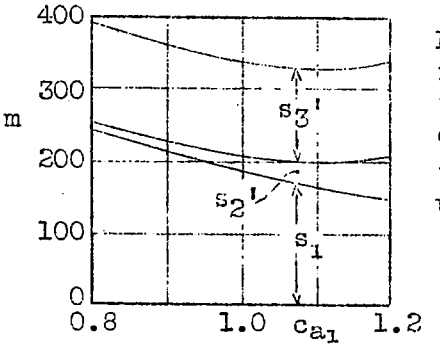

Figure 16.-Result of numerical example. The increase in the transition arc yields for $c_a = 1.1$ a minimum value for the total take-off distance up to an altitude of 20 m.